Interfacial rheology testing of molten polymer systems: Effect of molecular weight and temperature on the interfacial properties

Younes El Omari, Mohamed Yousfi, Jannick Duchet-Rumeau, Abderrahim Maazouz

Version of Record: https://www.sciencedirect.com/science/article/pii/S0142941821002294
Manuscript_dccac2d417907c4efdabab2ddca2b1c7

Interfacial rheology testing of molten polymer systems: effect of molecular weight and temperature on the interfacial properties

Younes El Omari[a*], Mohamed Yousfi[a*], Jannick Duchet-Rumeau[a] and Abderrahim Maazouz[a,b]

[a]Université de Lyon, INSA Lyon, CNRS, UMR 5223, Ingénierie des Matériaux Polymères, F-69621 Villeurbanne, France,
[b]Hassan II Academy of Science and Technology, Rabat, Morocco

[*]Corresponding author(s): younes.el-omari@insa-lyon.fr; mohamed.yousfi@insa-lyon.fr

Abstract:
The development of new interfacial rheological setup (IRS) for characterizing the interfacial viscoelastic properties of polymer systems is a subject of growing interest and constitutes a well-known challenge of high scientific and industrial application value. Recently, biconical and double-wall Ring (DWR) devices that can easily be attached to standard rheometers have been marketed for this purpose, but measurements must be made below 70 ° C to ensure a stable homogeneous temperature at the interface. Meanwhile each device has its own limitation: the bicone has high inertia and a relatively low Boussinesq number, giving it a low signal-to-noise ratio, while the DWR is too fragile to probe the interfaces of high viscous systems in the molten state. Currently, to predict the dynamic interfacial properties of molten polymer systems, the interfacial rheology characterization is based mainly on indirect methods such as numerical modelling. In this study, a novel high temperature resistant interfacial rheology cell has been developed. This new setup allows direct interfacial rheology measurements up to 200 °C with temperature gradients of 1 °C at the polymer-polymer interface. To validate this new IRS device, the surface/interfacial properties of different model fluids having different well-known structure and viscoelastic characteristics have been investigated. To enable a more sensitive measurement of interfacial rheological properties, lightweight titanium based biconical geometry was newly designed. The effect of the molecular weight and the temperature was highlighted. Finally, the interfacial rheology testing of molten semicrystalline polymer systems has been achieved for the first time. The measured apparent interfacial shear properties in both oscillatory and steady flow modes were carefully corrected, considering the contribution of the bulk-subphases during processing of the numerical data.

Keywords: interfacial shear rheology, interfacial tension, interface, interphase.

Introduction

Polymer systems are often made up of different macromolecular entities. They are seldom miscible with each other because of their high molecular weights and their high interfacial tension. When two immiscible polymers meet, a surface called an interface is created. This surface finds its thermodynamic origin in a positive free enthalpy of mixing related to the structural properties of the polymers. In particular, it is linked to the low entropy of the macromolecular chains and to the repulsive interactions between the two polymers. This two-dimensional area possesses different properties that are different from those of its two sub-phases. The interface formed which can be considered as being the third phase can be characterized not only by its interfacial tension but also by its intrinsic rheological properties that can potentially affect the resulting bulk properties. Interfacial properties have been demonstrated to control the morphology of polymer blends (dispersion of one polymer phase within another polymer matrix [1], multilayer coextruded polymers [2] and coalescence [3]), improve the stability of emulsions [4] and foams [5] and contribute usefully in other fields including crude oil recovery [6], cosmetic, biomedicine and food.

The interfacial rheology of two immiscible polymer systems is probed by investigating the response of the interface to an applied stress or strain according to the same formalism and techniques developed in the field of the bulk rheology [7]. In the two-dimensional rheology, we can distinguish between interfacial shear rheology and dilatational interfacial rheology. The difference between the two tests lies in whether or not the probed surface or interfacial area undergoes a change. Interfacial shear rheological measurements are often carried out using a rheometer and an interfacial geometry in order to shear the interface without modifying its area. The bicone [8, 9] is by far one of the most frequently used geometries for this purpose. It mimics the Couette device, but is much more tapered at its end **[10]**. The bicone has mainly been used in biology [11] or in oil extraction for studying the stability of emulsions [12] or for investigating the behavior of rigid interfacial layers between two immiscible fluids [13, 14]. The second interfacial geometry that we will consider here is the double wall ring (DWR) developed by *Vandebril et al*. [3]. Its geometry can be imagined as that of a double gap cylindrical Couette device. The double-wall ring has two gaps in which the interface is sheared. It consists of a thin ring and a cup (made of Delrin®, Teflon® or metal) with a rounded channel. The segment of the ring resembles a square allowing a better "grip" of the interface to the ring. The DWR is the most used interfacial shear rheology (ISR) geometry that is most used for measuring the interfacial viscoelasticity because of its low inertia and high sensitivity, especially for the study of low viscosity systems such as emulsions [3, 15], and foams [16].

In the ISR measurements, the optimization of the interface-to-bulk signal ratio is based on the maximization of the Boussinesq number (B_o) [17] given in equation 1.

$$B_o = \frac{\eta_s . P}{\eta_v . A} \qquad \text{(Equation 1)}$$

where η_s (Pa.s.m) is the surface viscosity in a steady shear flow that is calculated from the geometry adopted in the interfacial rheological measurements and from the measured torque; η_v is the bulk viscosity (Pa.s) = (η_1+ η_2) with η_1 and η_2 denoting respectively the viscosities of sub-phases 1 and 2; P is the contact perimeter between the shear geometry and the interface (m); and A is the contact area between the geometry and the surrounding sub-phases (m^2).

With regard to the measurements of the surface/interfacial rheology, it is worth mentioning that when the rheometer is going to measure the interfacial response (stress) toward an imposed strain, it also measures the response of the bulk sub-phases. Therefore, the deformation of the interface will unavoidably deform the two sub-phases that establish this interface. The measurement of the

interfacial rheological properties requires consideration of the relative contributions of the interfacial stress and the stress resulting from the surrounding bulk liquids. In other words, the Boussinesq number B_o allows the experimenter to predict if the contribution of the subphases to the interfacial response can be neglected or not.

If B_o is very low (<<1), the flow in the sub-phases can disturb the interfacial flow (significant fluid inertia) leading to an over estimation of the interfacial rheological properties [7]. In this case, corrections need to be applied to the measurable quantities in order to subtract the contributions of the sub-phases [18]. A numerical computation of the velocity profiles at the sub-phases and the interface, in different Boussinesq numbers and in the cylindrical coordinate system (r, θ, z) is used to solve the Navier-Stokes equation. The details of the corrections are explained in the references [7, 18]. For the DWR, the corrected values of the interfacial rheological quantities are obtained through an iterative approach (described in [18]). The algorithm is described in [18], and the codes implemented are available for download (https://softmat.mat.ethz.ch/opensource.html).

However, for the biconical geometry, the correction for the contributions of the sub-phases is integrated into the RheoCompass software using the equations of Oh and Slattery [7, 19]. There is also an algorithm described in the reference [11], and the codes implemented are available for download (https://data.mendeley.com/datasets/4tmy9k4ys3/1).

At the time of their preparation, processed polymer systems have the capacity to organize and form multi-scale structures. In the past, such preparation procedures were often conducted in the molten state, under high temperatures, high shear rate or under radiation (laser, UV, etc.). Nowadays, the 2D rheology measurements are conducted at ambient temperature bellow a maximum of 70°C. The experimental interfacial devices currently in the market are not suitable for measurements at high temperature or in the presence of highly viscous polymers. Until now, the interfacial rheological properties measurements carried out in the melt state have been based only on indirect experimental methods [20]. Moreover, other works have been focused on morphological and rheological modeling for accessing viscoelastic interfacial properties [21].

In the present work, two categories of polymer systems are studied. The first systems investigated consist of the interface formed between different model fluids that are liquid at room temperature. The effect of viscosities and elasticities of the sub-phases on the interfacial shear viscosity and interfacial shear modulus has been investigated by varying the molecular weights and the viscoelastic nature of the bulk components. The thermal dependence of the interfacial rheological parameters has also been studied by varying the temperature of the medium. The second systems investigated consist of molten immiscible thermoplastic polymers having different bulk viscosities. For the first time, a novel experimental interfacial setup dedicated to molten polymer systems is described. The interfacial rheological measurements at different temperatures are highlighted, and corrections of apparent data are considered and discussed.

Experimental

Materials and methods

Materials

The model fluids chosen are PDMS (Polydimethylsiloxane) trimethylsiloxy terminated supplied from abcr (and Alfa Acesar for the PDMS 3) and PIB (PolyIsobutene) supplied from INEOS. PDMS and PIB, used in the present work, present different molecular weights. Table 1 shows the composition of each materiel.

Table 1. Weight average molecular weight of the used PDMS and PIB.

Material	PDMS1	PDMS2	PDMS3	PDMS4	PDMS5	PIB1	PIB2	PIB3	PIB4	PIB5
Mw (g/mol)	5970	28000	63000	91700	204000	481	1333	1280	1440	3780

In this study, another grade of PDMS (From abcr, Mw= 410 g/mol)) and another grade of PIB (From INEOS, Mn=570 g/mol) have been used to sweep a very large range of PDMS and PIB viscosities.
For molten thermoplastic polymers, the PCL (polycaprolactone) and PEG (polyethylene glycol) are supplied from Sigma Aldrich and were chosen due to their low melting temperatures (around 70 °C). Different molecular weights of each polymer were used. Table 2 summarizes the characteristics of the polymers studied.

Table 2. Number average molecular weight of the polycaprolactone (PCL) and the polyethylene glycol (PEG) used.

Material	PCL1	PCL2	PEG1	PEG2	PEG3
Mn (g/mol)	10000	45000	10000	20000	35000

Characterization Methods

BULK RHEOLOGICAL MEASUREMENTS

In order to determine the rheological properties of different bulk subphases and their effect on the interfacial rheological measurements, dynamic rheological measurements were performed.
The first rheological tests on the model fluids were carried out on a DHR-2 machine from TA Instruments. i.e. a combined motor-transducer (CMT) rotational rheometer [22]. A cone-plate geometry was chosen (diameter 40 mm, angle 1.994. °) and the heating system used was a Peltier Plate temperature system. Frequency sweeps were performed at angular frequencies decreasing from 100 to 0.1 rad.s^{-1}. Complex viscosity ($|\eta^*|$) were measured as a function of the angular frequency.
In order to obtain more rheological data at high frequency, the time-temperature superposition principle was applied. The rheological curves obtained at different temperatures were superimposed on a reference curve (at a reference temperature T_0) by translating them using horizontal and vertical shift factors (log $a_{T/T0}$ and log $b_{T/T0}$ respectively). These factors depend mainly on the temperature T and the reference temperature T_0. In this study, the reference temperature chosen was 25°C. A strain sweep at an angular frequency of 100 rad/s was used to determine the linear viscoelastic range for each fluid.
The rheological behavior of PCL and PEG polymers was characterized using an ARES-G2 apparatus from TA Instruments, i.e. a separated motor-transducer (SMT) rheometer [23] that can alloy to attain a high shear rate up to 628 rad/s with negligible inertia effect. A parallel-plate geometry (of diameter 20 mm) was chosen and the heating used was a forced convection oven (FCO).

SURFACE AND INTERFACIAL TENSION MEASUREMENTS

The surface and interfacial tension at different temperatures were measured using an automatic drop tensiometer (TRACKER-H from Teclis Instruments, France). The main parts of the Tracker™ instrument are a light source, a CCD camera, a syringe holder system and a needle for drop formation. For an improved temperature control, a high temperature regulated view cell consisting of a stainless steel assembly with two sapphire windows was used. A thermocouple measures the temperature inside the cell. The entire assembly is surrounded by a plastic block made of PEEK. The high-temperature view cell could withstand a maximum temperature of 200 °C and a maximum pressure of 200 bar.
From the digital analysis of a melt or liquid drop, the profile was acquired by a high-speed CCD camera and characteristic surface parameters (area, volume, surface tension) were determined in real time. Surface tension was determined from the Tracker™ software which uses a special algorithm to

analyze the profile of the drop (either rising or pendant), and to fit it with models based on the Young-Laplace equation in order to determine surface tension, interfacial tension or contact angle [24, 25].

In theoretical terms, this method is based on the balance between the gravitational and surface tension forces according to the following equation

$$\boldsymbol{\gamma}\left(\frac{\mathbf{1}}{\boldsymbol{R_1}}+\frac{\mathbf{1}}{\boldsymbol{R_2}}\right)=\Delta\mathbf{P}=\Delta\mathbf{P_0}-\Delta\boldsymbol{\rho}\mathbf{gz} \qquad \text{(Equation 1)}$$

where $\boldsymbol{\gamma}$ is the surface/interfacial tension,

$\mathbf{R_1}$ and $\mathbf{R_2}$ are the first principal and second radius of curvature where:

$\Delta\mathbf{P}=\mathbf{P_{in}}-\mathbf{P_{out}}$ is the Laplace pressure, namely the pressure difference across the interface.

$\Delta\mathbf{P_0}$ is a reference pressure at z=0, whereas

$\Delta\boldsymbol{\rho}\mathbf{gz}$ is the hydrostatic pressure.

$\Delta\boldsymbol{\rho}=\boldsymbol{\rho_d}-\boldsymbol{\rho_c}$ is the density difference.

$\boldsymbol{\rho_d}$ and $\boldsymbol{\rho_c}$ are respectively the density of the drop phase and the density of the continuous phase.

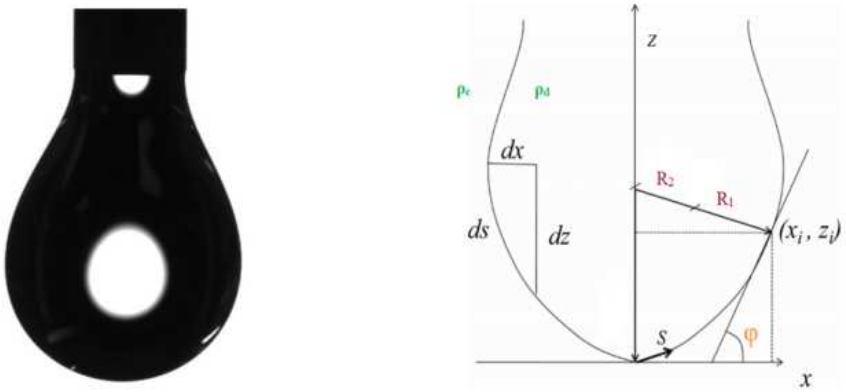

Figure 1. Image scan of the pendant drop (left). Schematic of the characteristics of the pendant drop (right).

The Bond number (Bd), which represents the ratio between the gravitational forces and the surface tension on an interface between two fluids, was carefully analysed prior to the measurements. To obtain high accuracy, the Bond number (B_d) was optimized that requiring an increase in the radius of curvature at the apex, which in turn, required an increase in the volume of the drop.

It is important to allow the drop liquid surface or fluid-fluid interfaces to achieve Laplace equilibrium before performing a measurement. When it comes to systems that are too liquid, this equilibrium is achieved rapidly (within a few seconds). On the contrary, when the polymer systems present a high bulk viscosity, the equilibrium state requires longer times (several hours).

MORPHOLOGICAL OBSERVATIONS

A polarized optical microscope (Zeiss, Germany) equipped with a sapphire hot stage was used to qualitatively probe the morphology of different PDMS-PIB model systems in isothermal conditions at 25 °C. The objective was to qualitatively check the compatibility of the studied systems. The preparation of PDMS-PIB blends (90/10 wt%) was performed using a dynamic rheometer (DHR2, TA Instruments) at a shear rate of 8 s^{-1} with a duration of 1250 seconds using a parallel-plate geometry (40mm) and a Peltier heating element to control the temperature at 25°C. High-quality images were taken with the aid of a scientific camera (Panthera 1M30).

To analyze the PCL-PEG morphology, scanning electron microscopy (SEM, HITACHI S-3500 N, Japan) was used at an accelerating voltage of 15 kV and a probe current of 130 pA. The PCL/PEG extrudates were cryofractured and coated with gold during 60 s at 2 kV before the SEM observations.
The immiscible PCL-PEG extrudate blends were prepared using a twin-screw DSM microcompounder. The temperature of melt mixing was 80°C, the screw velocity was 80 rpm and the residence time was five minutes.

NUMERICAL ASSESSMENT OF THE COMPATIBILITY OF THE POLYMER SYSTEMS STUDIED

To predict the compatibility of the systems studied, their Hansen' solubility parameters (HSP) were evaluated [26]. In the present work, we used HSPiP software (Louisville, Kentucky, USA) to evaluate the HSP. For the calculations, the software used a genetic algorithm optimization approach [27]. According to Hansen [28], the global solubility parameter is a combination of three components reflecting dispersive (London) (δ_D), polar (δ_P) and hydrogen bond (δ_H) interactions.

$$\boldsymbol{\delta^2 = \delta_{TOT}^2 = \delta_D^2 + \delta_P^2 + \delta_H^2} \qquad \text{(Equation 2)}$$

The determination of the Hansen solubility parameters of a polymer consists in testing the solubility of the polymer in different solvents with known solubility parameters using a sphere that encompasses the good solvents of the polymer in a 3D solubility diagram (δ_D, δ_P, δ_H), which defines as a solubility sphere with a radius R_0 [28, 29].
Polymers are expected to display a good mutual affinity when their HSPs are close and when the distance between the centres of their respective solubility spheres is low. The distance R_0 between centres of the solubility spheres of two components denoted 1 and 2 is given by:

$$\boldsymbol{R_0^2 = 4(\delta_{D1} - \delta_{D2})^2 + (\delta_{P1} - \delta_{P2})^2 + (\delta_{H1} - \delta_{H2})^2} \qquad \text{(Equation 3)}$$

We consider that two polymers would exhibit strong affinity in a presence of a very low value of Ra (inferior to R_0, the radius of the solubility sphere). However, when considering two different polymers, a value of $R_{0min} = 8$ MPa$^{1/2}$ is usually viewed as the upper limit for compatibility [28, 30].
To assist the software in optimizing its analysis of the HSPs, different fluids were drawn, and the solubility of the fluids was tested in various solvents in order to find a good solvent. The software made it possible to obtain an optimized 3D solubility diagram for the studied system studied.

INTERFACIAL RHEOLOGY

Interfacial rheological measurements with a double-wall ring (DWR) geometry

The first interfacial rheological tests on the model fluids were carried out on a DHR2 apparatus (TA Instruments) using a double-wall ring (DWR) geometry. The measuring range of the torque is 2 nN.m to 200 mN.m. The DWR is an association of two geometries, a biconical section to effectively catch and detect the interface (good grip and larger contact area) and a Du Noüy double air-gap ring geometry to reduce the meniscus during shear. The DWR geometry consists of three parts: the ring, the ring holder and the double air-gap cup, with the last item being placed on a Peltier plane that allows the cup to be heated (Figure 2). The geometrical characteristics of the used DWR geometry are summarized in Table 3. The ring and support feet are made of a platinum/iridium (Pt/Ir) composite that is characterized by its chemical inertness, ease of cleaning and wettability. The ring support is made of hardened steel. Significantly, the ring and the cup are perfectly adjusted (concentricity), and the cap placed on the Peltier plate is precisely levelled.

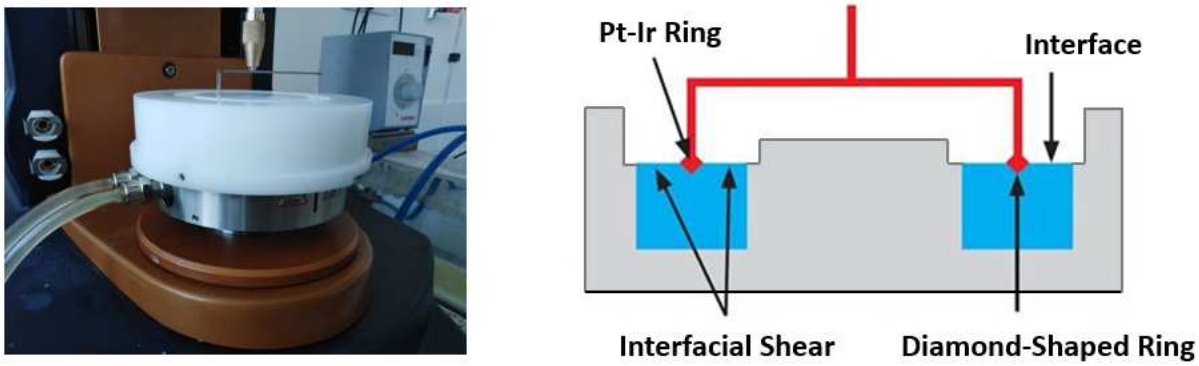

Figure 2. Photograph (left) and schematic diagram (right) of the double wall-ring cell.

The densest fluid was placed in the lower part of the cup. This volume corresponded to the internal air gap so that the possibility of having a meniscus was negligible. The ring was lowered at very low velocity until it came into contact with the surface of the first subphase. This step was carried out either visually or using normal force (the detection of the surface normal force depends on the surface tension of the liquid). The last step was to add the second sub-phase (the less dense phase) and rotate the ring (by two or three turns) to homogenize the interface.

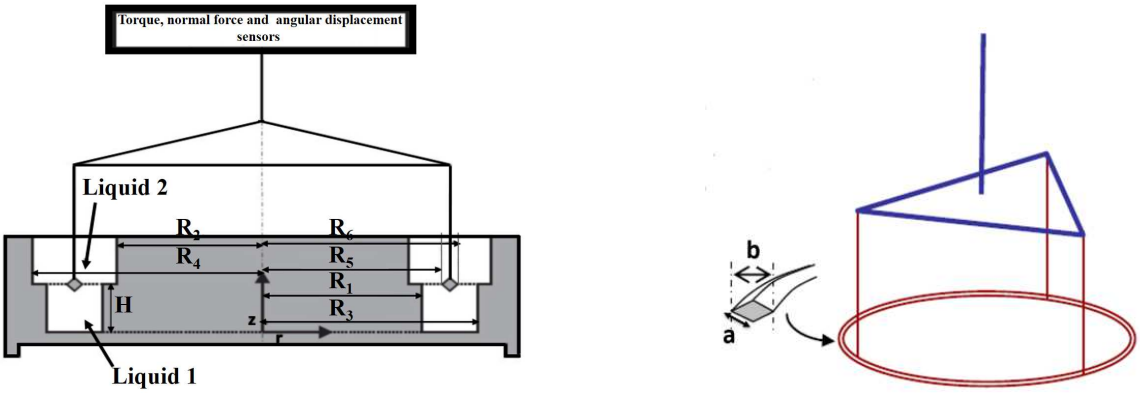

Figure 3. Schematic of the double-wall ring (DWR) device (left) [31] and schematic of the square section of the ring (DWR) (right).

Table 3: Dimensions of the DWR geometry.

R_1	R_2	R_3	R_4	R_5	R_6	b	a
(mm)	(mm)	(mm)	(mm)	(mm)	(mm)	(mm)	(mm)
31	34	35	39.5	34.5	35.5	1	0.7

The formula expressing the Boussinesq number in the DWR geometry is:

$$B_o = \frac{\eta_s}{\eta_v}\frac{1}{R_6 - R_5} = \frac{\eta_s}{\eta_v}\frac{1}{a} \qquad \text{(Equation 4)}$$

where **a** is the diameter of the wire of the ring (0.7 mm).
The expression of the interfacial viscosity when using the DWR is:

$$\eta_s = \frac{M}{2\pi(R_5^2+R_6^2)\left[\frac{1}{\left(\frac{R_5}{R_1}\right)^2-1}+\frac{1}{1-\left(\frac{R_6}{R_1}\right)^2}\right]\Omega} \qquad \text{(Equation 5)}$$

where **M**, and **Ω** are the measured torque and the angular velocity, respectively.

Corrections are carried out (based on a finite-difference calculation) for the sub-phase only for sensitive interfaces (when the interfacial viscosity and B_o are very low). The velocity profiles in the subphases can be determined by using the Navier-Stokes equation in cylindrical coordinates (R, θ, z). The boundary conditions include a no-slip condition at the inner and outer walls of the DWR trough as well as no-slip condition at the surface of moving ring [18].

And finally, the stress condition at the interface reduces to:

$$\eta_1 \frac{\partial v_1}{\partial z} - \eta_2 \frac{\partial v_2}{\partial z} = \eta_s \frac{\partial}{\partial r}\left(\frac{1}{r}\frac{\partial}{\partial r}(r.v_s)\right) \qquad \text{(Equation 6)}$$

As we said previously, the determination of the corrected interfacial viscosity is based on an iterative approach (see detail in the next paragraph) [18].

To that end, the expression of the calculated torque is given by:

$$M_c = 2.\pi.\eta_S.R\,\frac{3}{5}\,\frac{d}{dr}\left(\frac{v_s}{r}\right)\Big|_{r=R5} - 2.\pi.\eta_S.R\,\frac{3}{6}\,\frac{d}{dr}\left(\frac{v_s}{r}\right)\Big|_{r=R5} - 2.\pi.\eta_1.\int_{R_5}^{R_r}\frac{dv_1}{dp_1}\,r^2.dr - 2.\pi.\eta_1.\int_{R_r}^{R_6}\frac{dv_1}{dp2}\,r^2.dr - 2.\pi.\eta_2.\int_{R_5}^{R_r}\frac{dv_2}{dp_3}\,r^2.dr - 2.\pi.\eta_2.\int_{R_r}^{R_6}\frac{dv_2}{dp_4}\,r^2.dr \qquad \text{(Equation 7)}$$

The algorithm is described in [7], and the codes implemented are available for download (https://softmat.mat.ethz.ch/opensource.html).

Interfacial rheological measurements in steady flow and oscillation modes with DWR geometry are suitable for very fluid interfaces. However, this geometry has a limited usefulness for probing rigid interfaces or interfaces formed from highly viscous polymeric fluids. This is because the DWR geometry is a very fragile and can be deformed in the presence of rigid or very viscous materials. On the other hand, in the presence of such interfaces, a slip of the geometry with respect to the fixing rotation system is observed when the measured force increases sharply. For all these reasons, the interfacial rheological measurements for interfaces formed from high-viscosity fluids were performed using the biconical geometry which is much stiffer than DWR.

Interfacial rheological measurements with the biconical geometry

The bicone [11] is another geometry used for viscoelastic interfacial measurements. As mentioned above, it mimics the Couette device but is very tapered at its end (Figure 4). The biconical geometry was first patented by the Anton Paar Company [32].

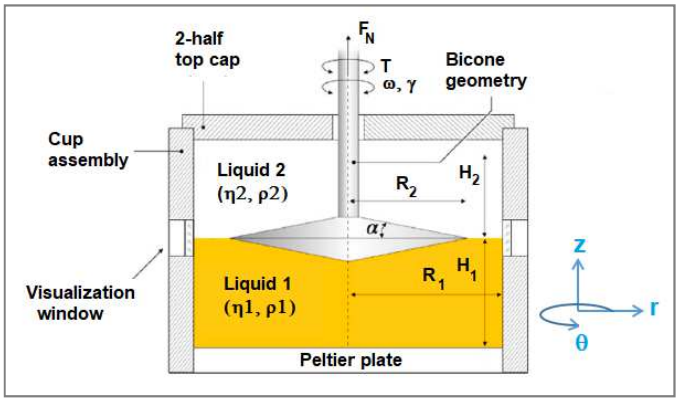

Figure 4. Schematic overview of the biconical interfacial rheometer [33].

The edges of the bicone are located on the interface between the two immiscible liquids. The biconical geometry can be also rotated or oscillated around its axis of rotation. In the following instance, the Boussinesq number will be expressed as:

$$\mathbf{B_o}=\frac{\eta_s}{\eta_1+\eta_2}\frac{\mathbf{1}}{R_b} \qquad \text{(Equation 8)}$$

where R_b is the radius of the bicone.

When Bo<<1, a numerical correction of the flow profile must be made in order to take into account the effects of the sub-phases and define the corrected value of the measured torque M_c (see the previous expressions) [18]. The algorithm is described in [11], and the codes implemented are available for download (https://data.mendeley.com/datasets/4tmy9k4ys3/1)

Without making these corrections, Oh and Slattery [9] deduced an exact solution to the velocity distribution in the two sub-phases and the interface. For both sub-phases, the authors assumed that mass and momentum were conserved [33]. In addition, the interface is specified to have the following features:

A jump mass balance at the interface: the dynamics of each of the two fluids is driven by the continuity and the Navier-Stokes equations in another words the velocity is continuous at the two-fluid interface.

$$\mathbf{div}\ \mathbf{v_\theta = 0} \qquad \text{with } \mathbf{v_\theta = v_s} \text{ (in the above Equation (7))} \qquad \text{(Equation 8)}$$

And a jump momentum balance at the interface: the balance between the pressure and bulk viscous stress jumps through the interface, the stress generated by surface intrinsic viscosity and elasticity and the stress resulting from dynamic surface tension, which includes equilibrium interfacial tension, Gibbs elasticity, and the Marangoni effect.

$$\boldsymbol{\tau_1.n_1+\tau_2.n_2+\ div(\tau)+\rho_s.g=0} \qquad \text{(Equation 9)}$$

where v_θ is the interfacial velocity vector, τ is the interfacial stress tensor, n_1 and n_2 are the normal vectors perpendicular to the interface pointing into phases 1 and 2, ρ_s is the mass density of the interface, and g is gravity per unit mass.

Oh and Slattery imposed the following boundary conditions:

- The sub-phases, as well as the interface, are incompressible and Newtonian.
- Supposing the interface is flat. the form and the velocity distribution of the interface are stationary (steady flow).
- Interfacial deflection is ignored. Therefore, the usual stress jump does not involve Laplace's pressure. The authors assume a low Reynolds number and neglect secondary flows.
- The interfacial mass balance simplifies the surface divergence term. There are no Marangoni effects in the tangential stress balance.
- The fluid velocity on the top, bottom and lateral of the walls is zero, while at the edge of the rotating bicone, it is equal to the velocity of the bicone.

Once this distribution of velocities is known, the reduced torque ($\overline{M}$) exerted by both liquids on the disk and the interface is determined according to:

$$\overline{M}=\overline{R_2}^3\,\mathbf{B_0}\frac{\partial}{\partial\bar{r}}\left(\frac{\overline{v_\theta}}{\bar{r}}\right)\Big|_{\bar{r}=\overline{R_2}}-\int_0^{\overline{R_2}}\frac{\partial\bar{v}_\theta^1}{\partial\bar{z}}\Big|_{\bar{z}=\overline{H_1}}\bar{r}^2\,\bar{r}\,\mathbf{dr}+\frac{1}{Y}\int_0^{\overline{R_2}}\frac{\partial\bar{v}_\theta^2}{\partial\bar{z}}\Big|_{\bar{z}=\overline{H_1}}\bar{r}^2\,\bar{r}\,\mathbf{dr} \qquad \text{(Equation 10)}$$

$$\mathbf{Y}=\frac{\eta_1}{\eta_2}\ ;\ \bar{r}=\frac{r}{R_1}\ ;\ \bar{z}=\frac{z}{R_1}\ ;\ \overline{H_1}=\frac{H_1}{R_1}\ ;\ \bar{v}_\theta^{\mathbf{j}}=\frac{v_\theta^j}{R_1\Omega-\bar{r}} \qquad \text{(Equation 11)}$$

The exact solution of the reduced torque $\overline{M}$ is:

$$\overline{M}=\frac{M}{2\pi\Omega\mathbf{R_1}^3(\eta_1+\eta_2)} \qquad \text{(Equation 12)}$$

In this case, we can just replace **M** by $\overline{M}$ in the expression giving the interfacial viscosity.

$$\eta_{s,corr}=\frac{1}{4\pi}\left(\frac{1}{R_1^2}-\frac{1}{R_2^2}\right).\frac{\overline{M}}{\Omega} \quad \text{(Equation 13)}$$

Oh and Slattery, experimentally established the following relation linking the torque and the Boussinesq number:

$$\overline{M}=\frac{2R_1^2}{R_2^2-R_1^2}B_0 \quad \text{(Equation 14)}$$

For rigid interfaces with a high Boussinesq number, the interfacial stress must be calculated when R_2 / H_1 and R_2 / R_1 tend towards 0.

$$M=\frac{8}{3}R_2^3(\eta_{1+}\eta_2)\,\Omega+4\pi R_2^2\,\eta_s\,\Omega \quad \text{(Equation 15)}$$

Interfacial viscosity will be expressed as:

$$\eta_s=\frac{M-\frac{8}{3}R_2^3(\eta_1+\eta_2)\,\Omega}{4\pi R_2^2\,\Omega} \quad \text{(Equation 16)}$$

It should be noted that a rheometer with a motor of low inertia cannot handle the biconical geometry because of its high weight (high momentum inertia). It is absolutely crucial to mention that characterizing a fluid interface (with low interfacial viscosity) is very difficult with the biconical geometry because the device is made from stainless steel; who suffers from high inertia and limited sensitivity.

For this reason, in this work, a novel biconical geometry was manufactured from titanium (Ti) instead of stainless steel. This titanium-based geometry is roughly half as dense as its stainless-steel equivalent but presents the same shape and dimensions.

This novel biconical geometry was designed by the Anton Paar Research and Development Service (Stuttgart, Germany) (D: 68.28 mm, angle 5°). Its composition of titanium material (ρ= 4.506 g/cm^3) made it less dense than the previous bicone (steel, ρ= 7.5 to 9 g/cm^3) and therefore provided it with the beneficts of decreased inertia (denoted I) and increased its sensivity. This new Ti bicone which was attached to an MCR 302 rheometer was used for the very first time in this study. The inertia of Titanium based bicone geometry (0.0143 mN.m.s^2) is lower than stainless steel one (0.0227 mN.m.s^2).

Note that in interfacial rheological measurements with low-viscosity fluids, the experiment is performed in the limit of rheometer performance (Torque limit). Thus, a small improvement in the inertia value is beneficial for accuracy of measurements.

As mentioned above, the geometric ratio of the DWR is high which in turns leads to a high value of Boussinesq number value compared to the bicone. That said, in the field of polymer, the Boussinesq number is not the only parameter we need to consider. Due to the high viscosity of polymers, the stiffness of the geometry is also an important variable to consider. For this reason, the Ti bicone was used for rigid systems, whereas the DWR was used for fluid systems.

In this study, PIB-PDMS interfaces in addition to air-PIB and air-PDMS surfaces were investigated. The surfaces (air-fluid) and interfaces (fluid-fluid) that were studied are summarized in table 4.

Table 4: Model fluid surfaces and interfaces

Surfaces	Air-PDMS2 Air-PIB2	Air-PDMS3 Air-PIB3	Air-PDMS4 Air-PIB4	Air-PDMS5 Air-PIB5
Interfaces	PIB2-PDMS2	PIB3-PDMS3	PIB4-PDMS4	PIB5-PDMS5

Note that the sub-phases have the same range viscosity values.

Before moving on the interfacial rheological measurements, the miscibility of the different model fluid systems was checked using the optical microscopy and the calculated solubility parameters.

Novel experimental setup for interfacial rheological measurements of molten polymer systems

In order to study the interfaces between two molten polymers at high temperature, a novel interfacial rheology setup was manufactured. The novel interfacial rheology system (IRS) is equipped with a Peltier Plate temperature device (P-PTD 200) combined with an Anton Paar patented actively heated hood (H-PTD200). The Peltier-temperature-controlled hood allows interfacial rheological measurements up to 200 °C and results in temperature gradients of 1 °C at the sample interface. The interfacial geometry is the biconical titanium–based measuring system described above which is used in conjunction with a novel homemade IRS cell.
To withstand high measurement temperatures, the cylindrical cup cell was manufactured entirely from stainless-steel contrary to the cup currently marketed by the Anton Paar Company. The latter consists of an assembly of a metallic, glass, thermoplastic polymers and elastomeric ring components
The interfacial cell contains a threaded hole with a sealed screw that allows the introduction of the upper subphase fluid into the cup (Figure 5).

Figure 5. The newly designed interfacial rheology setup, shown in open position (left) and in closed position (right).

A normal force assisted surface detection methodology was used to accurately position the titanium-based biconical geometry at the fluid-fluid interface. The rheometer's interfacial analysis software (RheoCompass), based on the unique Navier-Stokes solution of the full flow field for a biconical geometry (see details in the introduction of this paper) was used to calculate of the corrected interfacial rheological properties.

Results

Model fluids investigation

Bulk rheological characterization

The bulk rheological data of different model fluids were evaluated from the master curves obtained using the time-temperature superposition principle. The main objective was to determine their rheological behaviour, over a large frequency domain. The latest data were used to define the viscous properties of PDMS and PIB subphases and their effect on the interfacial rheological measurements. The master curves corresponding to each PDMS and PIB model fluids are presented in the supporting information (Appendix 1). It was observed that PIB and PDMS fluids exhibit Newtonian behaviour

until an angular frequency of 1000 rad/s is reached. The Newtonian viscosities of the different model fluids are summarized in the Table 5.

Table 5. The zero-shear viscosity of the model fluids at 25°C.

	Newtonian viscosity (Pa.s) at 25°C		
PIB1	0.2	PDMS1	0.1
PIB2	2.9	PDMS2	1.0
PIB3	8.9	PDMS3	10.3
PIB4	17.9	PDMS4	26.4
PIB5	289.5	PDMS5	269.7

It is useful to note that the zero-shear viscosities will be used to subtract the effects of the sub-phases effects. This information is used as input data to correct for the effects of the subphases.
The Van-Gurp-Palmen plot [34] (δ (°) as a function of the complex modulus $G^*(\omega)$) was used to probe the chain structure of the studied polymers.

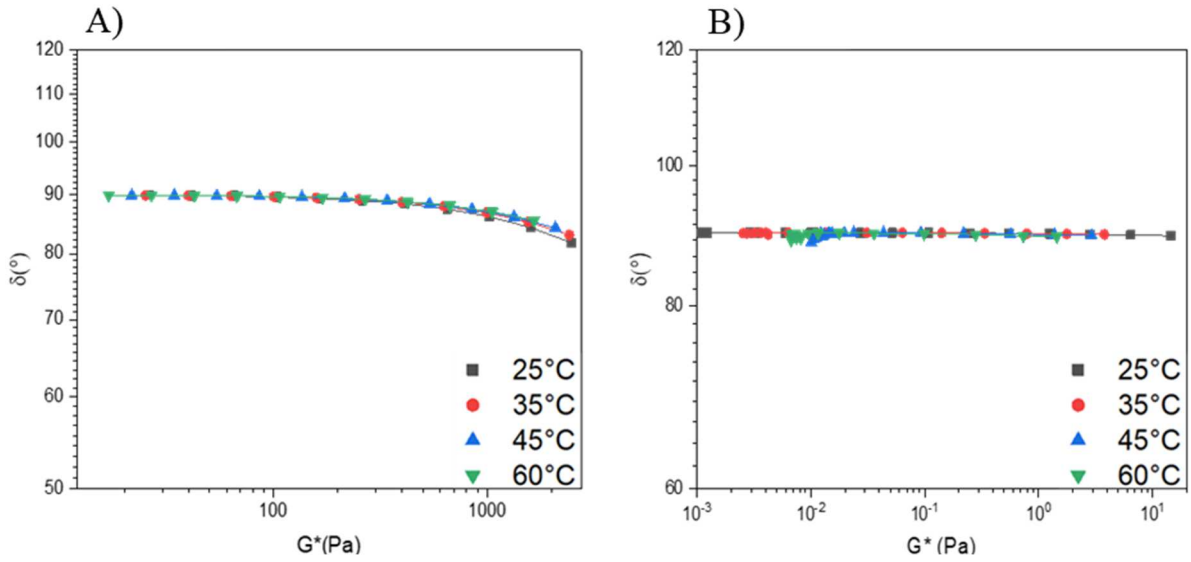

Figure 6. Variation of the phase-shift angle as a function of the complex modulus for PDMS4 (A) and PIB4 (B) at 25°C, 35°C, 45°C and 60°C.

From Figure 6 one can deduce that the variation of the phase-shift angle δ (°) as a function of the complex modulus $G^*(\omega)$ for the PDMS4 and PIB5 is independent of the temperature. Therefore, these fluids are thermo-rheologically simple. The Van-Gurp-Palmen plot corresponding to the other PDMS and PIB model fluids are presented in the supporting information (Appendix 1). These observations demonstrate the validity of the time-temperature superposition curves obtained. On the other hand, the Van-Gurp Palmen plots for the PDMS and PIB polymers display a classic shape that is generally expected for linear polymers with a plateau of the phase angle at 90° in the low frequency zone, indicating viscous behaviour in this Newtonian zone. At higher frequencies or higher complex moduli, the phase angle decreases. *Trinkle et al*. [35] have obtained such typical plots for linear polyethylene.

Surface tension

The experimental results for the measurements of surface tension obtained for the different grades of PDMS and PIB are shown in Figure 7.

It can be seen that the surface tension of the model fluids decreases when the temperature increases [36]. On the other hand, the surface tension increases with the growth of the viscosity. In fact, the more the viscosity increases the more material is cohesive and the more the energy of attraction between the macromolecules that oppose the surface break increases (more spherical drop shapes).

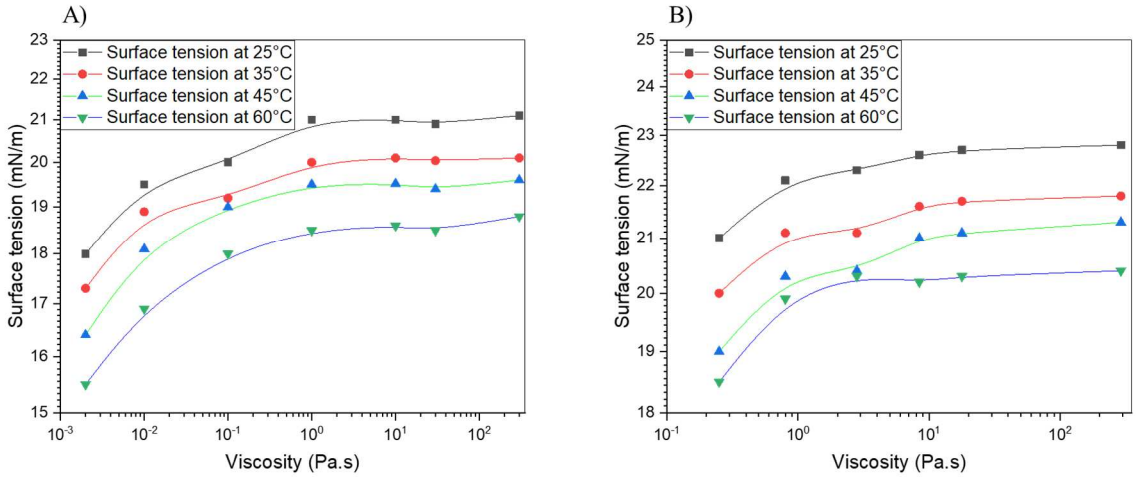

Figure 7. Evolution of the surface tension of the model fluids (PDMS (A) & PIB (B)) as a function of temperature and viscosity.

The same tendency was found by *Cazaux et al*. [37] in the case of PA66. They observed that the surface tension decreases when the molecular weight decreases according to the LeGrand and Gaines model [38]. The authors found that the surface tensions of polymer liquids vary with molecular weight according to an empirical relationship:

$$\gamma = \gamma_{\infty} - \frac{k}{M^{\frac{2}{3}}} \qquad \text{(Equation 23)}$$

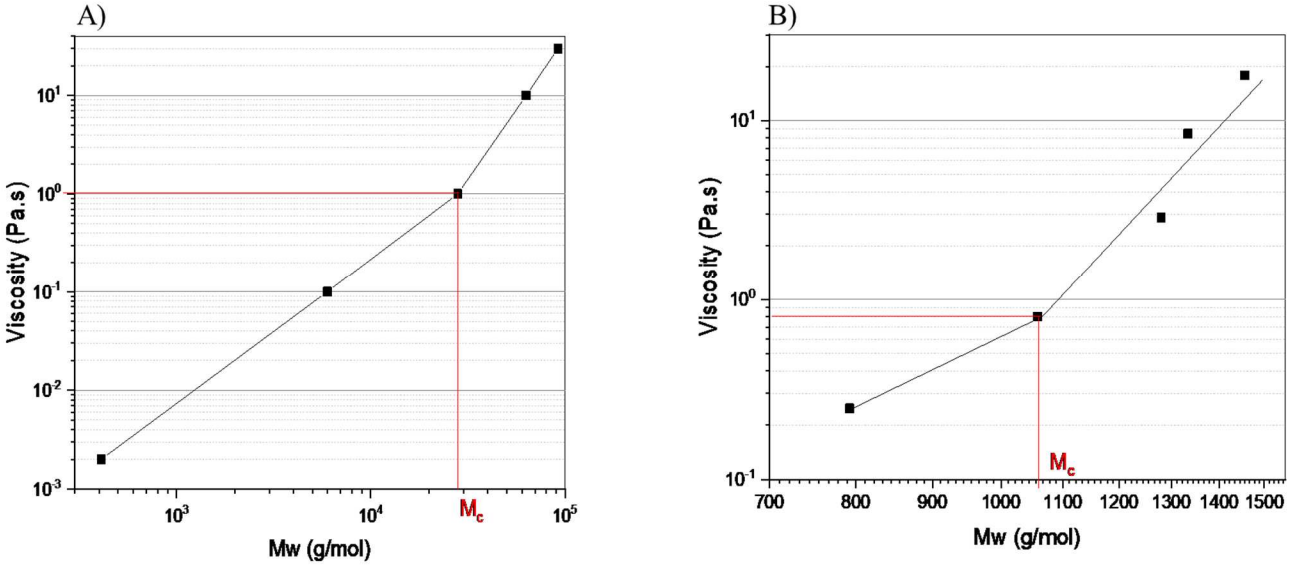

Figure 8. Variation of the viscosity of the model fluids (PDMS (A) & PIB (B)) as a function of their molecular weights.

We note that the sudden change in the trend of variation in surface tension as a function of viscosity (Figure 8) is related to the M_c (critical molecular weight) in both PDMS and PIB. Indeed, Figure 8

shows that the M_c corresponds to a viscosity of 1 Pa.s in PDMS samples and 0.80 Pa.s in PIB samples. On the other hand, the temperature coefficient of surface tension of PDMS and PIB varies with the viscosity along a similar trend to the surface tension and shows an abrupt change at a viscosity of 1 Pa.s (for PDMS) and 0.80 Pa.s (for PIB), which corresponds to the value of M_c. After this molecular weight, the surface tension does not change, tending toward constant value γ_∞.

Optical microscopy

Figure 9 shows the optical images of the model fluids studied. Droplets of PIB in the PDMS matrix are clearly seen. A well-defined interface between the PIB nodules and the PDMS matrix is clearly identified. The diameter of the PIB droplets increases when their viscosities increase, which reflect the behavior of immiscible or partially miscible liquids. Similar trends were found by Tong et al. in similar systems **[39]** in which PDMS and PIB were not miscible over the composition range investigated.

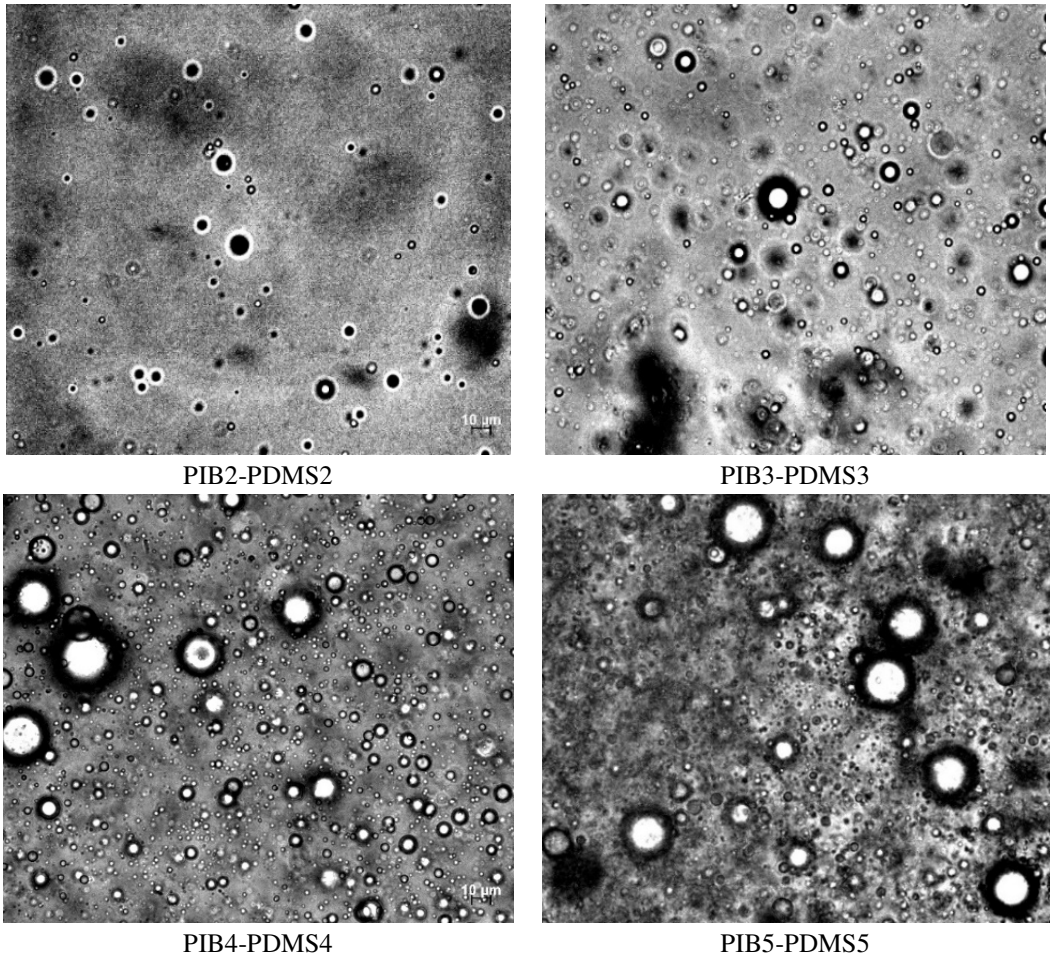

PIB2-PDMS2 PIB3-PDMS3

PIB4-PDMS4 PIB5-PDMS5

Figure 9. Morphology corresponding to 10-wt.% PIB in PDMS matrix at a shear rate of 8 s^{-1} for 1250s.

Solubility parameters

From the HSHiP software analysis, the Gibbs free energy of mixing is positive regardless of the polymer volume fraction (blue curve). Also, the second derivative of the Gibbs free energy is negative (red curve). Therefore, the systems studied are partially miscible, confirming the optical microscopy and SEM analysis results. Furthermore, the distance R_a between the centres of the solubility spheres is equal to 2.87 $MPa^{1/2}$ which is lower than the critical distance R_{0min}. The theoretical solubility

parameters of the PIB & PDMS obtained by HSHiP software are summarized in the supoorting informations (Appendix 4)

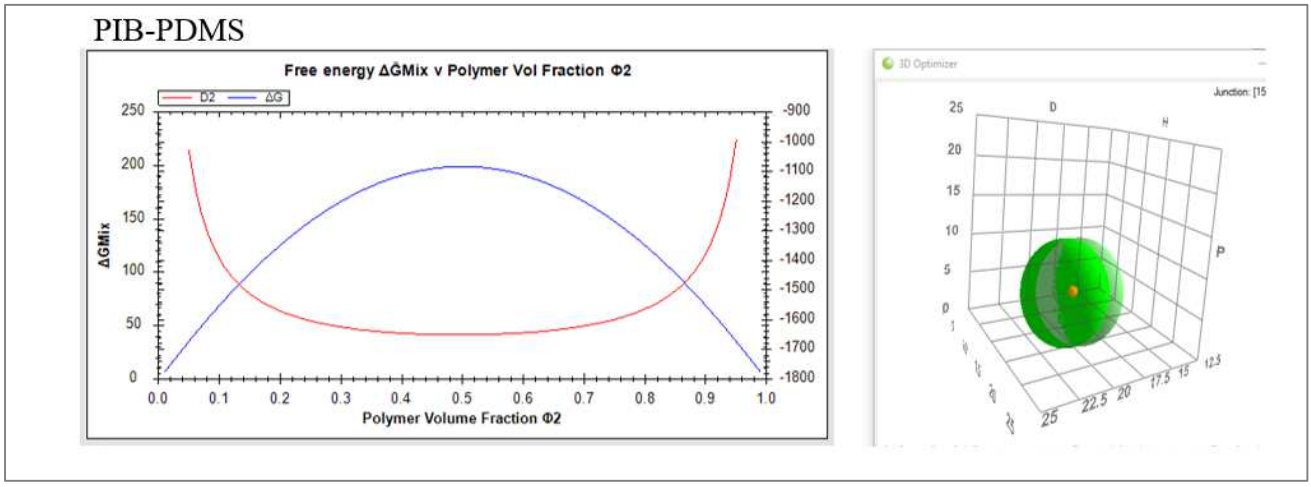

Figure 10. the Gibbs free energy of mixing of the PIB-PDMS & PEG-PCL systems.

Interfacial rheology

For each surface and interface, the experiments were performed as follows. First, the linear region was defined by an amplitude sweep experiment, and then the frequency and steady flow sweep tests were carried out. The effect of the temperature on the interfacial properties was also evaluated. Finally, a correction for the contribution of the sub-phases was performed to extract the real interfacial and surface properties.

Surface responses

Only the Ti bicone were used in this part. For the air-PDMS surface, we present just one system (air-PDMS3) using the test previously described (Figure 11). For the other air-PDMS surfaces, the details are presented in the Supporting Information.

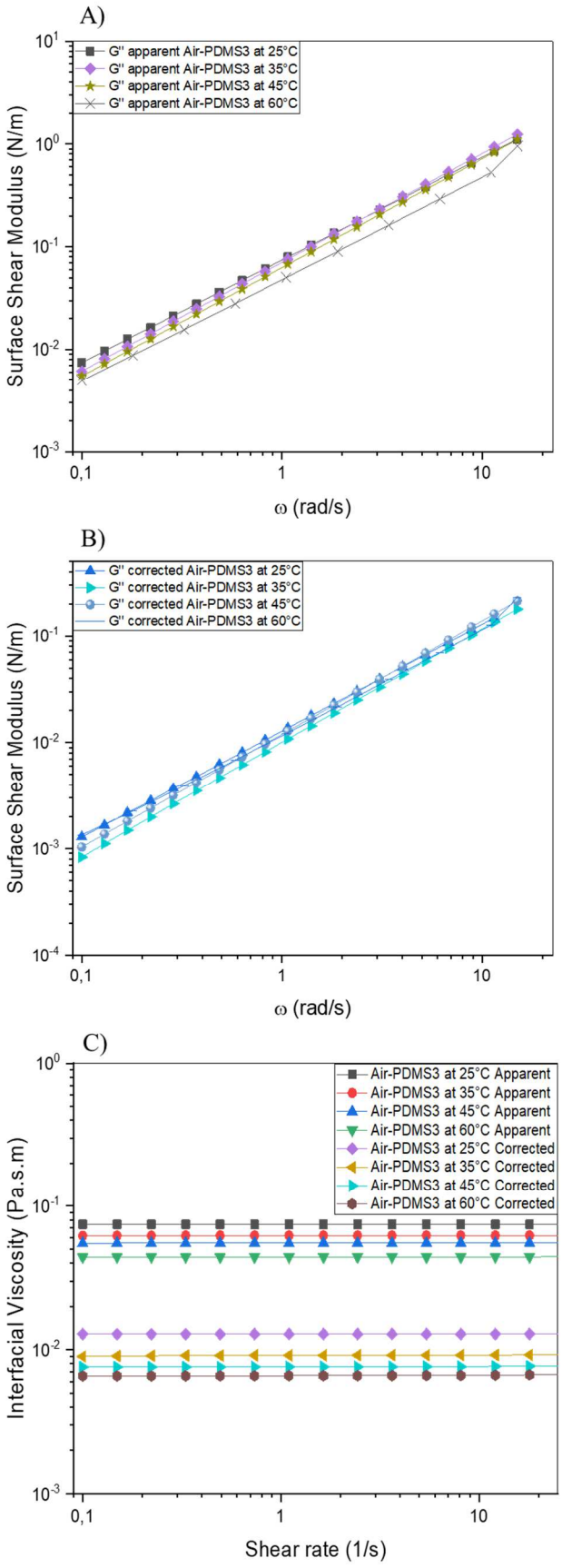

Figure 11. Frequency sweep (apparent modulus (A), corrected modulus (B)) and the steady shear (C) experiments of air-PDMS3 surface.

From the frequency sweep test, it can be seen that the air-PDMS3 surface exhibits viscous behaviour because no elasticity is detected. When the temperature increases, the apparent surface loss modulus G" decreases as well. After the correction for the subphase effect in the oscillatory test, the same tendency is observed. There are no data collected at the temperature of 25°C due to the high inertia of the subphase and also due to the bicone inertia because of its high weight, and thus it was not straightforward to carry out a dynamic test (frequency sweep). For the flow sweep, we note that this surface is Newtonian. The corrected surface viscosity increases when the fluid bulk viscosity increases. The bicone could apply a permanent flow sweep (just a simple rotation contrary to the back and forth motion of the frequency sweep test). The same tendency was found for the other surfaces. Table 6 summarizes the surface viscosities of the different surfaces at 60°C.

Table 6. Surface shear properties of the air-PDMS surfaces at 60°C.

Surface	Apparent surface viscosity (Pa.s.m) at 60°C	Boussinesq Number at 60°C	Corrected surface viscosity (Pa.s.m) at 60°C	Temperature effect on the surface viscosity
Air-PDMS2	$4.1.10^{-3}$	0.20	$3.6.10^{-4}$	↓↓↓↓
Air-PDMS3	$4.4.10^{-2}$	0.21	$5.5.10^{-3}$	↓↓↓↓
Air-PDMS4	0.13	0.23	$2.0.10^{-2}$	↓↓↓↓
Air-PDMS5	1.3	0.62	0.69	↓↓↓↓

As shown in Table 6, the Boussinesq numbers at 60°C are deficient because of the high viscosity of the subphases. Thus, carrying out these corrections is of primordial importance. We can also see that the viscosity of the surface increases when the viscosity of the subphases increases. This phenomenon is likely related to the cohesion of chain layers at the surface due to the viscosity effect which is in agreement with to the definition of the surface based on the Boussinesq approach [17, 40]. The latter imagines the surface as a superposition of layers with variable density; this density gradient gives enough force to the fluid to maintain it in a fixed range. Similar trends were observed in the air-PIB.
For the interfacial rheological measurements of the other air-PIB surfaces at different temperatures, the plot details are presented in the Supporting Information (Appendix 2).

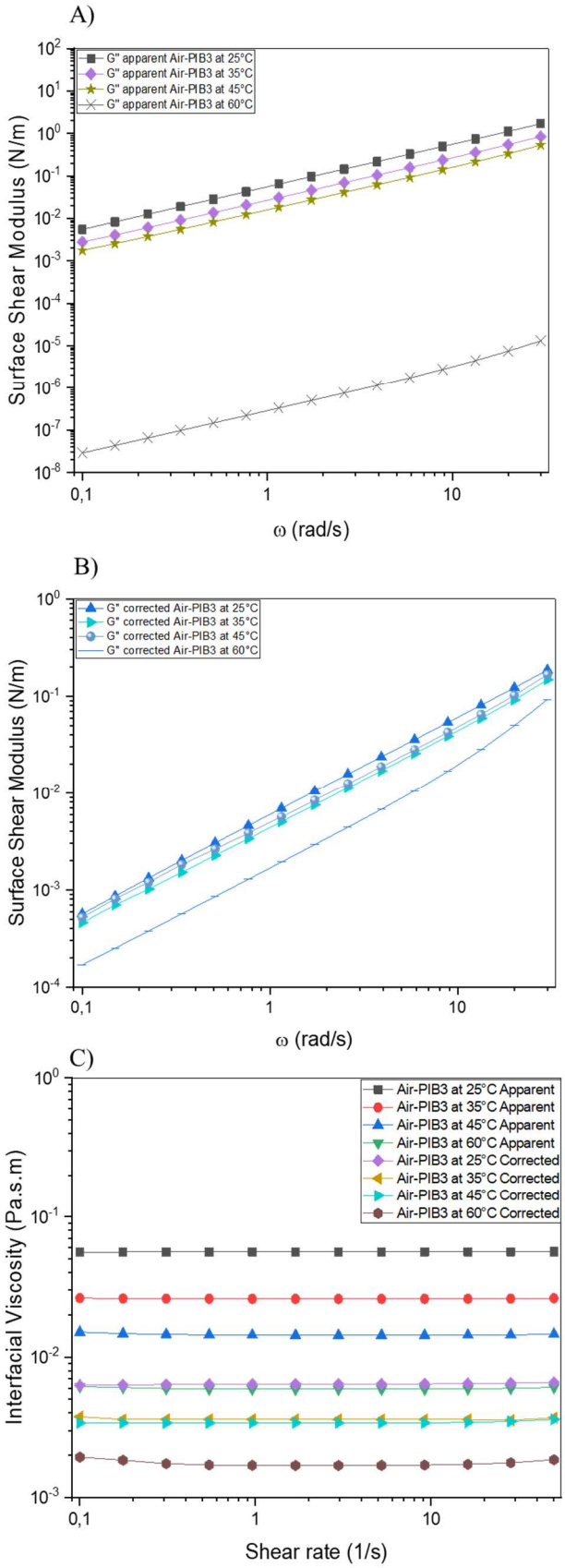

Figure 12. Frequency sweep (apparent modulus (A), corrected modulus (B)) and the steady shear (C) experiments of air-PIB3 surface.

Table 7. The interfacial shear properties of Air-PIB surfaces at 60°C.

Surface	Apparent surface viscosity (Pa.s.m) at 60°C	Boussinesq Number at 60°C	Corrected surface viscosity (Pa.s.m) at 60°C	Temperature effect on the surface viscosity
Air-PIB2	$2.9.10^{-3}$	0.28	$1.9.10^{-4}$	↓↓↓↓
Air-PIB3	$6.1.10^{-2}$	0.30	$0.9.10^{-3}$	↓↓↓↓
Air-PIB4	$3.1.10^{-2}$	0.60	$4.9.10^{-2}$	↓↓↓↓
Air-PIB5	0.23	0.30	0.1	↓↓↓↓

Interface responses

In this section, the DWR geometry was used to characterize the interfaces between high melt flow rate fluid subphases (PIB2-PDMS2) and the titanium biconical geometry for the interfaces between highly viscous subphases (PIB3-PDMS3, PIB4-PDMS4 and PIB5-PDMS5). (see Figure 13 and 14)

In the case of the PIB2-PDMS2 system, the interface is purely viscous (Newtonian behavior). It is useful to indicate that no elastic modulus was detected. According to *Läuger et al.* [41], the absence of a measurable modulus of elasticity in the case of ultra-high melt flow rate liquids could be due to the torque sensitivity limit of the rheometer being reached. In these conditions, the inertia of the geometry and the instrument exceeds the response of the interface.

On one hand, we can observe that, for a fixed temperature, both the apparent and corrected interfacial viscosities increase when the viscosity of the subphases increases. On the other hand, the apparent and corrected interfacial moduli (and the interfacial viscosity) decrease when the temperature increases. However, for PIB3-PDMS3 interface, the relationship between the apparent and the corrected interfacial magnitudes does not undergo the same trend. The apparent data obtained show that the interfacial viscous modulus G" decreases when the temperature increases, in contrast to the corrected values of the effects of the subphases when is subtracted (very low Boussinesq numbers). These interfaces remain Newtonian, but the interfacial viscosity increases due to the rise of the temperature. The same observation applies to the other interfaces (PIB4-PDMS4 and PIB5-PDMS5). For the other fluid-fluid interfaces, all figures were presented in the Supporting Information (Appendix 3). Table 8 summarizes the interfacial viscosities of these systems.

A)

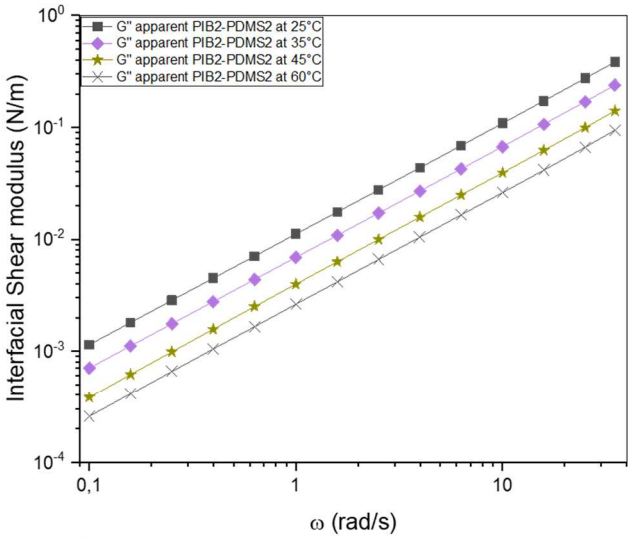
G'' apparent PIB2-PDMS2 at 25°C
G'' apparent PIB2-PDMS2 at 35°C
G'' apparent PIB2-PDMS2 at 45°C
G'' apparent PIB2-PDMS2 at 60°C
Interfacial Shear modulus (N/m)
ω (rad/s)

B)

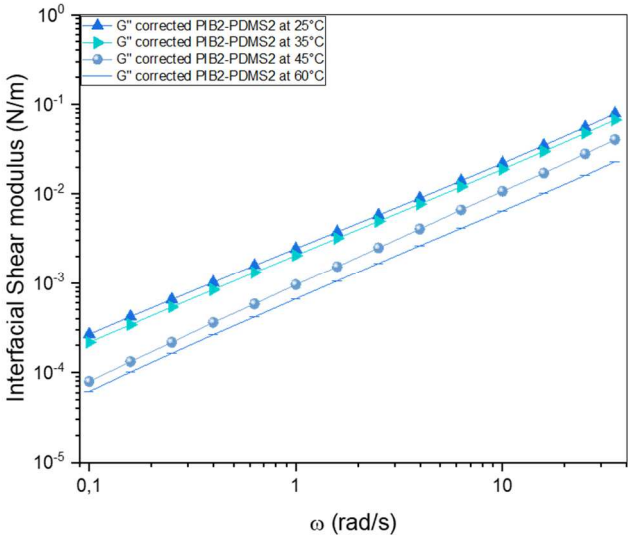
G'' corrected PIB2-PDMS2 at 25°C
G'' corrected PIB2-PDMS2 at 35°C
G'' corrected PIB2-PDMS2 at 45°C
G'' corrected PIB2-PDMS2 at 60°C
Interfacial Shear modulus (N/m)
ω (rad/s)

C)

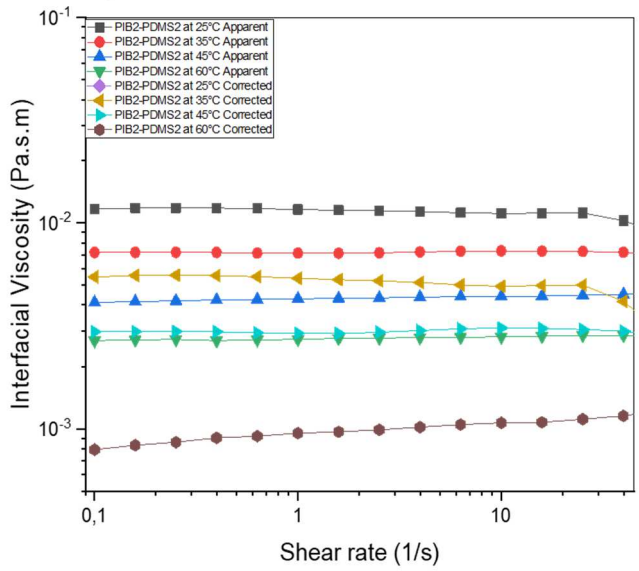
PIB2-PDMS2 at 25°C Apparent
PIB2-PDMS2 at 35°C Apparent
PIB2-PDMS2 at 45°C Apparent
PIB2-PDMS2 at 60°C Apparent
PIB2-PDMS2 at 25°C Corrected
PIB2-PDMS2 at 35°C Corrected
PIB2-PDMS2 at 45°C Corrected
PIB2-PDMS2 at 60°C Corrected
Interfacial Viscosity (Pa.s.m)
Shear rate (1/s)

Figure 13. Frequency sweep (apparent modulus (A), corrected modulus (B)) and the steady shear (C) experiments of the PIB2-PDMS2.

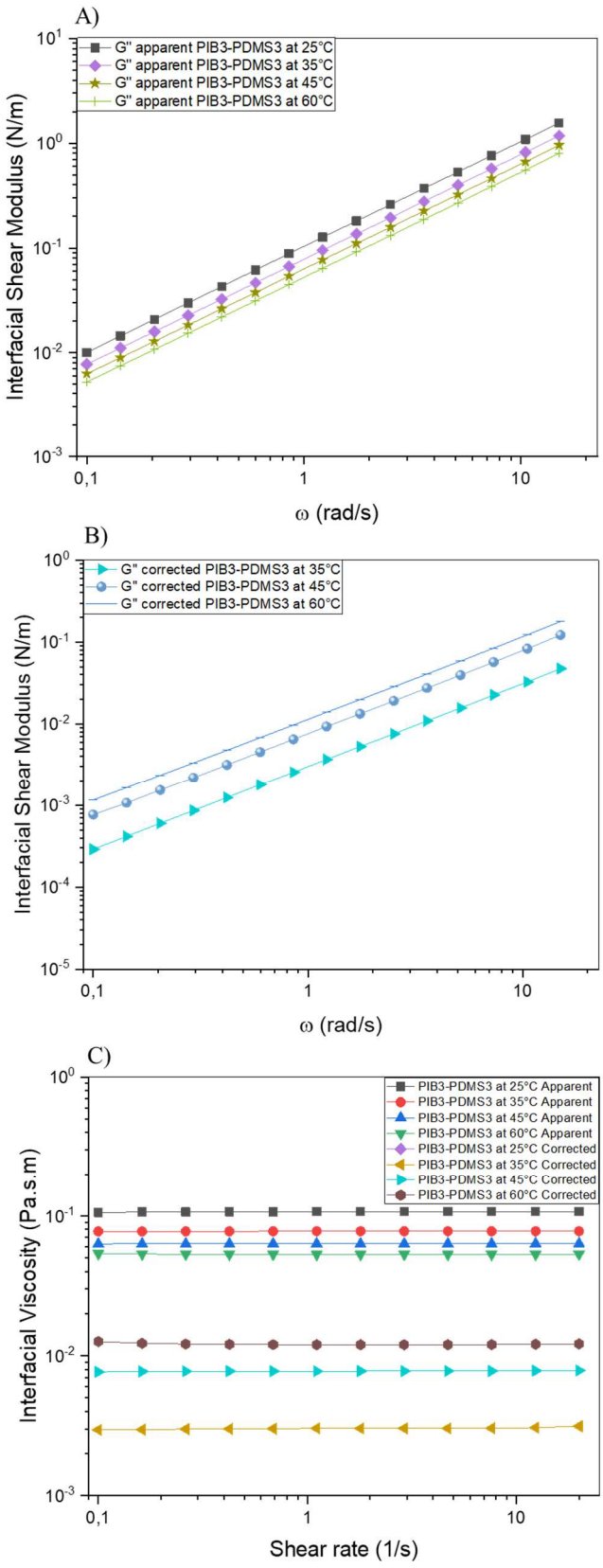

Figure 14. Frequency sweep (apparent modulus (a), corrected modulus (b)) and the steady shear (c) experiments of the PIB3-PDMS3 interfaces.

Table 8. Interfacial shear properties of the PIB-PDMS interfaces at 60°C.

Interface	Apparent interfacial viscosity (Pa.s.m) at 60°C	Boussinesq Number at 60°C	Corrected interfacial viscosity (Pa.s.m) at 60°C	Temperature effect on the interfacial viscosity
PIB2-PDMS2	$2.71.10^{-3}$	4.30	$1.02.10^{-3}$	↓↓↓↓
PIB3-PDMS3	$5.37.10^{-2}$	0.24	$1.26.10^{-2}$	↑↑↑↑
PIB4-PDMS4	0.13	0.21	$2.69.10^{-2}$	↑↑↑↑
PIB5-PDMS5	1.27	0.30	$5.47.10^{-1}$	↑↑↑↑

From Table 8, it can be seen that from a known molecular weight of the sub-phases, an increased temperature leads to increased interfacial viscosity, the macromolecules are long enough to diffuse from one phase to the other, and we no longer refer to an interface but to an interphase (Figure 15). As we mentioned earlier in the section dealing with the solubility parameters, the PIB and PDMS are partially miscible. Raising the temperature may lead to an increase in the miscibility. The small macromolecules migrate from one phase into the other by crossing the interface. In other words, the increased temperature makes it possible to boost the intra-entanglement at the interface and an interphase is formed.

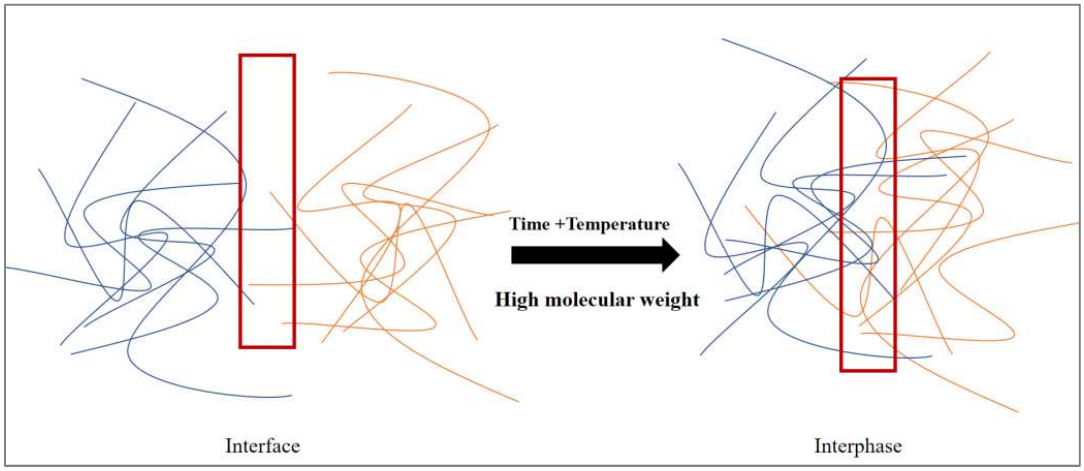

Figure 15. Transition from the interface to the interphase

Similar observations were reported by Tufano *et al.* [42] in the case of PIB-PDMS systems. They studied the diffusion from the light subphase to the heavy subphase ($Mn_{PIB} < Mn_{PDMS}$) at the interface by measuring the evolution of interfacial tension as a function of the temperature [42]. Table 9 summarizes the effect of the temperature on the interfacial tension in the case off the PIB-PDMS systems considered in this study.

Table 9. Effect of temperature on the interfacial tension of the PDMS-PIB systems studied.

Interface	γ(mN/m) at 25°C	γ(mN/m) at 35°C	γ(mN/m) at 45°C	γ(mN/m) at 60°C
PIB2-PDMS2	2.15	2.3	2.4	4.2
PIB3-PDMS3	2.8	2.6	2.2	1.9
PIB4-PDMS4	2.9	2.6	2.5	2.1
PIB5-PDMS5	3.8	2.9	2.8	2.3

For the PIB2-PDMS2 system, the PIB2 drop becomes more and more spherical within the PDMS2 due to the temperature increase. The interface between the two subphases becomes less stable (which explains why the interfacial shear viscosity decreases with increasing temperature). On the contrary,

for the other interfaces, the drop grows to be extended which increases the contact area between the subphases and creates interphases.

Molten polymer systems investigation

Scanning Electron Microscopy

Figure 16 shows the SEM images of PCL-PEG blends of different grades. A nodular morphology is observed regardless of the viscosity ratio used which indicates once again the presence of a partially miscible polymer structure over the composition range studied [43].

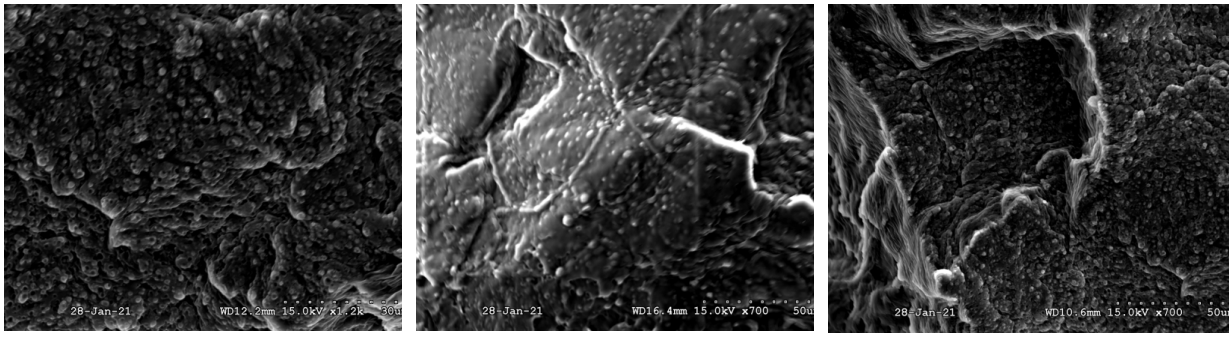

PCL1-PEG1 PCL2-PEG2 PCL3-PEG3

Figure 16. Morphology corresponding to PCL/PEG extrudates.

Solubility parameters

For this system, the HSHiP software allowed to the distance Ra between the centres of the solubility spheres is equal to 3 $MPa^{1/2}$ which is lower than critical distance R_{0min}. Thus the PCL-PEG systems are partially miscible.

Interfacial Shear rheology of molten polymer systems

The interfacial rheological measurements of the PCL-PEG systems should be made far from their crystallization temperatures. Thus, to measure the melting and crystallization temperatures of the PCL and PEG polymers. The crystallization and melting temperatures are very close (see Appendix 5 in the supporting information). Therefore, the shear interfacial rheological properties of PCL-PEG molten systems were examined at temperatures higher than 80 °C to prevent the crystallization of the subphases.

In this section, interfaces in the molten state between two highly crystalline polymers (PEG/PCL systems) were investigated based on the interfacial shear rheology. Because of the high viscosity of the melt polymers, the titanium bicone was used to probe the interfaces.

The bulk rheological curves (master curves at the reference temperature of 90°C) are depicted in Supporting Information part. It was observed that the two semi-crystalline polymers (PCL and PEG) are Newtonian in the shear rate region studied.

The interfacial properties of three different systems (PCL1-PEG1, PCL1-PEG2 and PCL2-PEG3) were studied from the steady shear experiments at 90 °C, 100 °C and 110°C.

Because of the high rigidity of their subphases, the interfacial shear properties of the PEG-PCL systems were examined using the titanium bicone. The steady flow tests show that all the interfaces are Newtonian. The apparent interfacial viscosities for each PEG-PCL system decrease when the temperature increases but different trends for the corrected values after correcting for the effects of the sub-phases.

For the PCL1-PEG1 system, increasing the temperature leads to a decrease in the interfacial viscosity. Otherwise, the interfacial viscosity of the PCL1-PEG2 and PCL2-PEG3 systems increases when the

temperature increases (the same observation can be made with the interfacial loss modulus) (See figures 17 & 18). The actual results are similar to those found previously with PIB-PDMS systems. Because of the partial miscibility between the PEG and the PCL and from a specific molecular weight, the interface turns into an interphase.

An attempt was made to measure the interfacial tension between PCL and PEG at different temperatures using the pendant drop method. Unfortunately, these tests were unsuccessful for two essential reasons. The first reason was due to the difference in density between the two polymers which is almost zero, preventing the application of the Laplace law. The second reason was the refractive index difference which was close, therefore inducing a low optical contrast.

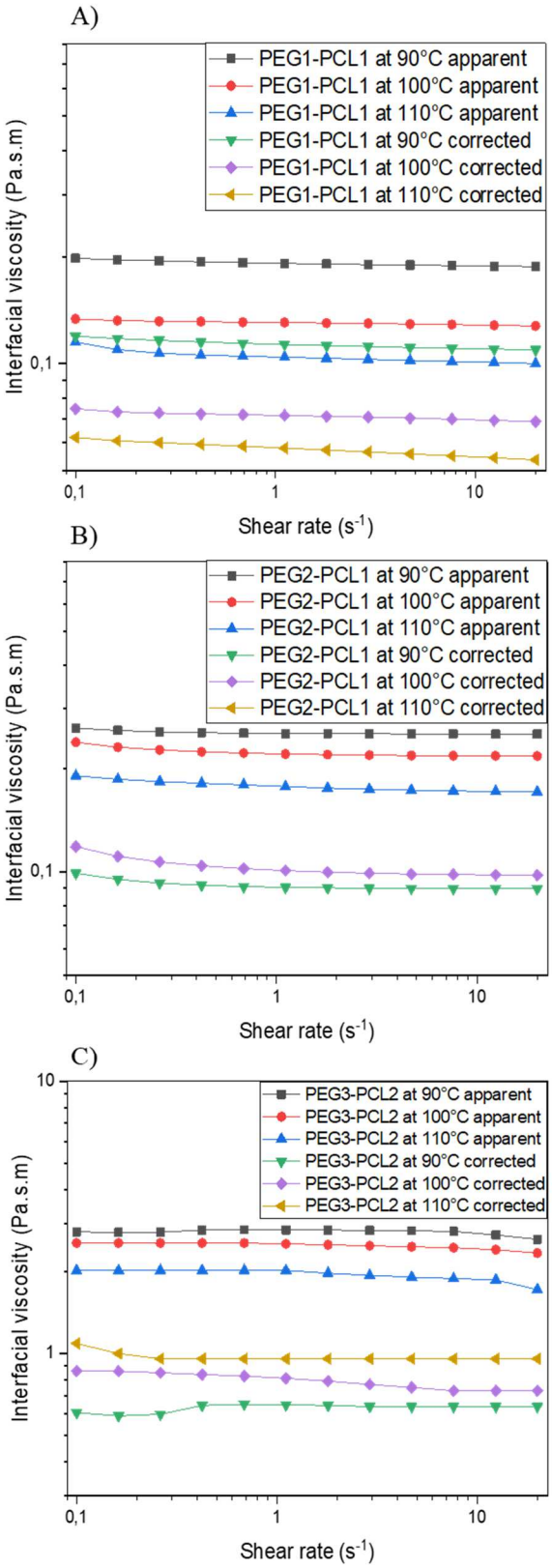

Figure 17. Variation of the interfacial shear viscosity with the angular frequency of PEG/PCL systems (PEG1-PCL1 (A), PEG2-PCL1 (B) & PEG3-PCL2 (C)).

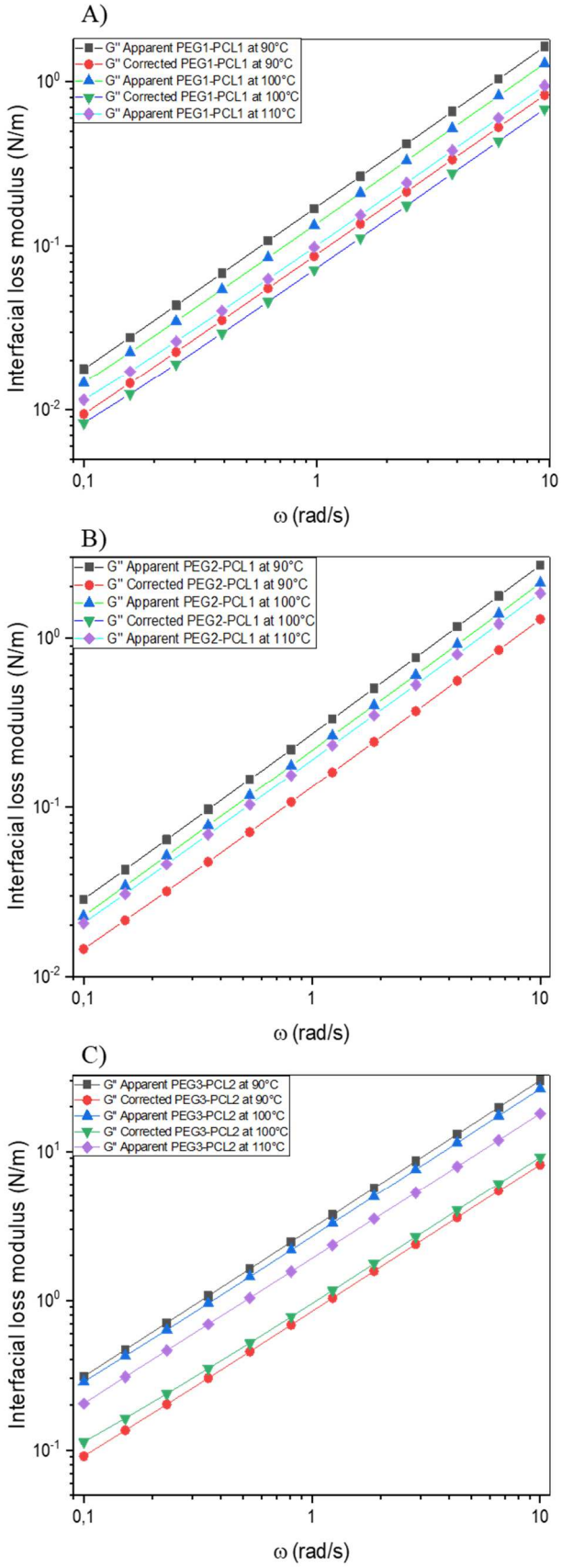

Figure 18. Variation of the interfacial shear loss modulus with the angular frequency of the PEG/PCL systems (PEG1-PCL1 (A), PEG2-PCL1 (B) & PEG3-PCL2 (C))..

Table 10. Effect of the temperature on the interfacial tension of studied PCL/PEG systems.

Interface	Apparent interfacial viscosity (Pa.s.m) at 90°C	Boussinesq Number at 90°C	Corrected interfacial viscosity (Pa.s.m) at 90°C	Temperature effect on the interfacial viscosity
PCL1/PEG1	0.19	0.44	0.12	↓↓↓↓
PCL1/PEG2	0.26	0.36	0.10	↑↑↑↑
PCL2/PEG3	2.8	0.30	0.60	↑↑↑↑

Conclusions

The present work highlights the implementation of two rheological tools for characterizing the interfacial shear rheology of polymer systems. The measurements with the DWR setup showed a limiting subphase viscosity of 3 Pa.s when probing the interfaces from high melt flow rate liquids. Otherwise, a slip of the geometry with respect to the fixing rotation system was observed.

In the case of air/fluid surfaces, purely viscous behaviour was noticed. The corrected surface viscosity increased when the fluid bulk viscosity increased. As for the interfacial investigation of PIB-PDMS systems, the interface was purely viscous (Newtonian behavior). At a constant temperature, the more the viscosity of the subphases increased, the more the interfacial viscosity increased. On the other hand, for low-viscosity fluid systems, both the apparent and corrected interfacial moduli (and the interfacial viscosity) decreased when the temperature increased. However, when the interfaces were formed from a highly viscous fluid medium, the corrected interfacial viscosity underwent an opposite trend with the rise of the temperature indicating the formation of an interphase.

The measurements in the molten state of PCL-PEG systems using the newly developed biconical IRS showed that starting from a specific molecular weight, the interface turned into an interphase which inducing an increase in interfacial viscosity.

The results of this study could be transposed for the probing of other immiscible thermoplastic polymers that exhibit more complex interfaces such as in the presence of solid nanofillers, compatibilizers or multilayers.

Acknowledgments

The authors are indebted to Murat Arli (INSA Lyon) in his help for the design of interfacial rheological cell and thank Dr. Yves Chevalier (Claude Bernard University Lyon 1) for the stimulating discussions. The authors are thankful to David Duval, Mr Georg Krennfrom, Mr Markus Thiele and Dr. Joerg Laeuger (Anton Paar Gmbh) for their recommendations and technical assistance regarding the interfacial rheological measurements with the bicone. The authors also gratefully acknowledge Thibault Tavernier and David Israel for their helpful discussion and training on the use of the DWR setup. Finally, the authors also gratefully acknowledge the French Ministry of Superior Education and Research (MESRI) for the doctoral study grant.

References

[1] M. Yousfi, T. Dadouche, D. Chomat, C. Samuel, J. Soulestin, M.F. Lacrampe, P. Krawczak, Development of nanofibrillar morphologies in poly(l-lactide)/poly(amide) blends: role of the matrix elasticity and identification of the critical shear rate for the nodular/fibrillar transition, Rsc Advances 8(39) (2018) 22023-22041.

[2] B. Lu, A. Bondon, I. Touil, H. Zhang, P. Alcouffe, S. Pruvost, C. Liu, A. Maazouz, K. Lamnawar, Role of the Macromolecular Architecture of Copolymers at Layer–Layer Interfaces of Multilayered Polymer Films: A Combined Morphological and Rheological Investigation, Industrial & Engineering Chemistry Research (2020) 22144-22154 .
[3] S. Vandebril, J. Vermant, P. Moldenaers, Efficiently suppressing coalescence in polymer blends using nanoparticles: role of interfacial rheology, Soft Matter 6(14) (2010) 3353-3362.
[4] J.S. Hong, P. Fischer, Bulk and interfacial rheology of emulsions stabilized with clay particles, Colloids and Surfaces A: Physicochemical and Engineering Aspects 508 (2016) 316-326.
[5] D. Langevin, Influence of interfacial rheology on foam and emulsion properties, Advances in Colloid and Interface Science 88(1-2) (2000) 209-222.
[6] H.-Q. Sun, L. Zhang, Z.-Q. Li, L. Zhang, L. Luo, S. Zhao, Interfacial dilational rheology related to enhance oil recovery, Soft Matter 7(17) (2011) 7601-7611.
[7] D. Renggli, A. Alicke, R.H. Ewoldt, J. Vermant, Operating windows for oscillatory interfacial shear rheology, Journal of Rheology 64 (2020) 141-160.
[8] J.L. Grossiord, A. Ponton, La mesure en rhéologie: des avancées récentes aux perspectives, Les Ulis: EDP Sciences 1(2013) 1-365.
[9] O. Soo-Gun, J.C. Slattery, Disk and biconical interfacial viscometers, Journal of Colloid and Interface Science 67(3) (1978) 516-525.
[10] S. Derkach, J. Krägel, R. Miller, Methods of measuring rheological properties of interfacial layers (Experimental methods of 2D rheology), Colloid journal 71(1) (2009) 1-17.
[11] P. Sánchez-Puga, J. Tajuelo, J.M. Pastor, M.A. Rubio, Dynamic measurements with the bicone interfacial shear rheometer: Numerical bench-marking of flow field-based data processing, Colloids and Interfaces 2(4) (2018) 69-86.
[12] P.A. Rühs, C. Affolter, E.J. Windhab, P. Fischer, Shear and dilatational linear and nonlinear subphase controlled interfacial rheology of β-lactoglobulin fibrils and their derivatives, Journal of Rheology 57(3) (2013) 1003-1022.
[13] Y. Fan, S. Simon, J. Sjöblom, Interfacial shear rheology of asphaltenes at oil–water interface and its relation to emulsion stability: Influence of concentration, solvent aromaticity and nonionic surfactant, Colloids and Surfaces A: Physicochemical and Engineering Aspects 366(1-3) (2010) 120-128.
[14] L.M. Ligiero, C. Dicharry, N. Passade-Boupat, B. Bouyssiere, P.M. Lalli, R.P. Rodgers, C. Barrère-Mangote, P. Giusti, P. Bouriat, Characterization of crude oil interfacial material isolated by the wet silica method. part 2: Dilatational and shear interfacial properties, Energy & Fuels 31(2) (2017) 1072-1081.
[15] S. Barman, G.F. Christopher, Simultaneous interfacial rheology and microstructure measurement of densely aggregated particle laden interfaces using a modified double wall ring interfacial rheometer, Langmuir 30(32) (2014) 9752-9760.
[16] S. Costa, R. Höhler, S. Cohen-Addad, The coupling between foam viscoelasticity and interfacial rheology, Soft Matter 9(4) (2013) 1100-1112.
[17] L.E. Scriven, Dynamics of a fluid interface equation of motion for Newtonian surface fluids, Chemical Engineering Science 12(2) (1960) 98-108.
[18] S. Vandebril, A. Franck, G.G. Fuller, P. Moldenaers, J. Vermant, A double wall-ring geometry for interfacial shear rheometry, Rheologica Acta 49(2) (2010) 131-144.
[19] J.C. Slattery, L. Sagis, E.-S. Oh, Interfacial transport phenomena, Springer Science & Business Media (2007).
[20] I. Delaby, B. Ernst, R. Muller, Drop deformation during elongational flow in blends of viscoelastic fluids. Small deformation theory and comparison with experimental results, Rheologica Acta 34(6) (1995) 525-533.
[21] D. Graebling, R. Muller, J. Palierne, Linear viscoelastic behavior of some incompatible polymer blends in the melt. Interpretation of data with a model of emulsion of viscoelastic liquids, Macromolecules 26(2) (1993) 320-329.
[22] D. Merger, M. Wilhelm, Intrinsic nonlinearity from LAOStrain—experiments on various strain- and stress-controlled rheometers: a quantitative comparison, Rheologica Acta 53(8) (2014) 621-634.

[23] A. Franck, Measuring Structure of Low Viscosity Fluids in Oscillation Using a Rheometer with and without Separate Torque Transducer, ANNUAL TRANSACTIONS-NORDIC RHEOLOGY SOCIETY 11 (2003) 95-100.
[24] J.D. Berry, M.J. Neeson, R.R. Dagastine, D.Y. Chan, R.F. Tabor, Measurement of surface and interfacial tension using pendant drop tensiometry, Journal of colloid and interface science 454 (2015) 226-237.
[25] Y. Rotenberg, L. Boruvka, A. Neumann, Determination of surface tension and contact angle from the shapes of axisymmetric fluid interfaces, Journal of colloid and interface science 93(1) (1983) 169-183.
[26] H. CM, Hansen solubility parameters: a user's handbook, Florida: CRC (2007).
[27] M.D. de los Ríos, E.H. Ramos, Determination of the Hansen solubility parameters and the Hansen sphere radius with the aid of the solver add-in of Microsoft Excel, SN Applied Sciences 2(4) (2020) 1-7.
[28] C.M. Hansen, The universality of the solubility parameter, Industrial & engineering chemistry product research and development 8(1) (1969) 2-11.
[29] C.M. Hansen, The three dimensional solubility parameter, Danish Technical: Copenhagen 14 (1967).
[30] R. Gallu, F. Méchin, F. Dalmas, J.-F. Gérard, R. Perrin, F. Loup, On the use of solubility parameters to investigate phase separation-morphology-mechanical behavior relationships of TPU, Polymer 207 (2020) 122882.
[31] A. Franck, Double Wall Ring Geometry to Measure Interfa-cial Rheological Properties, APN031, TA Instruments, Germany (2015) 1-9.
[32] P. Bohr, H. Stettin, J. Läuger, Biconical geometries in rheometers: Exact solution for the flow field and implications for the design of measuring systems, Review of Scientific Instruments 90(1) (2019) 015114.
[33] P. Erni, P. Fischer, E.J. Windhab, V. Kusnezov, H. Stettin, J. Läuger, Stress-and strain-controlled measurements of interfacial shear viscosity and viscoelasticity at liquid/liquid and gas/liquid interfaces, Review of scientific instruments 74(11) (2003) 4916-4924.
[34] S. Trinkle, C. Friedrich, Van Gurp-Palmen-plot: a way to characterize polydispersity of linear polymers, Rheologica Acta 40(4) (2001) 322-328.
[35] S. Trinkle, P. Walter, C. Friedrich, Van Gurp-Palmen plot II–classification of long chain branched polymers by their topology, Rheologica Acta 41(1-2) (2002) 103-113.
[36] E. Mezger, Loi de variation de la tension superficielle avec la température J. Phys. Radium 10 (1946), 303-309.
[37] G. Cazaux, Faisabilité des procédés LCM pour l'élaboration de composites renfort continu à matrice thermoplastique polyamide, Doctorat d'Université, Le Havre, 2016.
[38] D. LeGrand, G. Gaines Jr, The molecular weight dependence of polymer surface tension, Journal of Colloid and Interface Science 31(2) (1969) 162-167.
[39] W. Tong, Y. Huang, C. Liu, X. Chen, Q. Yang, G. Li, The morphology of immiscible PDMS/PIB blends filled with silica nanoparticles under shear flow, Colloid and Polymer Science 288(7) (2010) 753-760.
[40] S. Nguyen, Dynamique d'une interface en présence d'une singularité de contact solide/fluide, Doctorat d'Université Paris Sud XI (2005) 211p.
[41] J. Läuger, A new rheometer platform for extended testing capabilities, Annual transactions of the Nordic rheology society 21 (2013) 1-5.
[42] C. Tufano, G. Peters, P. Van Puyvelde, H. Meijer, Transient interfacial tension and morphology evolution in partially miscible polymer blends, Journal of colloid and interface science 328(1) (2008) 48-57.
[43] K. Ragaert, G. Maeyaert, C. Martins, L. Cardon, Bulk compounding of PCL-PEO blends for 3D plotting of scaffolds for cardiovascular tissue engineering, Journal of Materials Science and Engineering 3(1) (2014) 1-4.